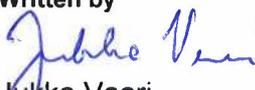
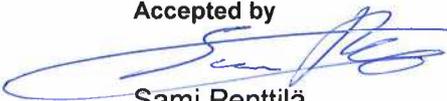
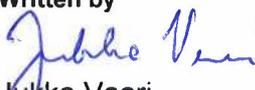
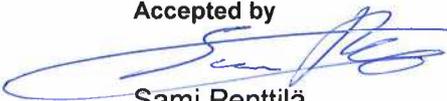
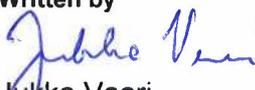
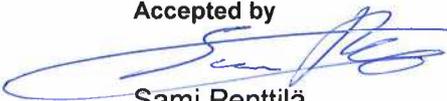


# Review on NDTs detecting ageing induced changes in polymer structures

Authors: Jari Rinta-Aho, Konsta Sipilä, Jukka Vaari

Confidentiality: Public

<b>Report's title</b> Review on NDTs detecting ageing induced changes in polymer structures				
<b>Customer, contact person, address</b> SAFIR2022	<b>Order reference</b>			
<b>Project name</b> Safety criteria and improved ageing management research for polymer components exposed to thermal-radiative environments	<b>Project number/Short name</b> 121248/SAMPO			
<b>Author(s)</b> Jari Rinta-Aho, Konsta Sipilä, Jukka Vaari	<b>Pages</b> 19			
<b>Keywords</b> Nuclear power plant cables, polyethylene, cross linked polyethylene, non-destructive evaluation, ageing, molecular dynamics simulations	<b>Report identification code</b> VTT-R-00074-20			
<b>Summary</b> <p>In nuclear power plants (NPP) there can be 1000-2000 km of cables as part of various instrumentations. The condition of the cables becomes more critical as NPPs age, especially in such cases, when the original lifetime of a plant is planned to be extended. Thus there is a demand for reliable and non-destructive condition monitoring techniques in ageing management of cables. The adapted research philosophy in this project is to combine computational modelling and experimental testing to find correlations between the ageing induced changes in the studied material and non-destructively measured material parameters. Finding such correlations would ease setting an acceptance criterion for the studied materials. Thus, various non-destructive techniques (NDT), such as DSC, infrared / Raman spectroscopy, NMR, ultrasonic and dielectric spectroscopy, were examined in order to identify the ability of molecular dynamics (MD) simulations to predict the measurement parameters of each NDT when PE and XLPE are studied. It seemed that the measurement parameters provided by ultrasonic technique could be estimated by MD simulations. Sound velocities for PE and XLPE could be estimated based on the extracted Young's modulus, Poisson's ratio, density and bulk modulus values by using MD simulations. However, the estimated sound velocity values seemed to be lower than the values reported in literature. Possible explanations for the lower values may be related to extraction of Young's modulus and Poisson's ratio values, as the calculated sound velocity is sensitive to changes in these parameters. Future work is focused on examining the reasons why the produced sound velocities vary from the measured ones and how ageing will effect to the sound velocity predictions.</p>				
<b>Confidentiality</b>	Public			
Espoo 23.1.2020 <table border="0" style="width: 100%;"> <tr> <td style="width: 33%; vertical-align: top;"> <b>Written by</b>              Jukka Vaari,            Senior Scientist         </td> <td style="width: 33%; vertical-align: top;"> <b>Reviewed by</b>              Timo Saario            Principal Scientist         </td> <td style="width: 33%; vertical-align: top;"> <b>Accepted by</b>              Sami Penttilä            Research Team Leader         </td> </tr> </table>		<b>Written by</b>  Jukka Vaari, Senior Scientist	<b>Reviewed by</b>  Timo Saario Principal Scientist	<b>Accepted by</b>  Sami Penttilä Research Team Leader
<b>Written by</b>  Jukka Vaari, Senior Scientist	<b>Reviewed by</b>  Timo Saario Principal Scientist	<b>Accepted by</b>  Sami Penttilä Research Team Leader		
<b>VTT's contact address</b> P.O.Box 1000. FI-02044 VTT, Finland				
<b>Distribution (customer and VTT)</b> SAFIR one copy, VTT one copy				
<i>The use of the name of VTT Technical Research Centre of Finland Ltd in advertising or publishing of a part of this report is only permissible with written authorisation from VTT Technical Research Centre of Finland Ltd.</i>				

## Preface

---

This work was completed as part of the SAFIR2022 –research program in SAMPO (Safety criteria and improved ageing management research for polymer components exposed to thermal-radiative environments) project’s Work Package 2 ”Improvements in ageing management of polymer components”, Task 2.3 “Improved interpretation of non-destructive testing data”.

Espoo 23.1.2020

Authors

## Contents

---

Preface.....	2
Contents.....	3
1. Introduction.....	4
2. Methods.....	5
2.1 Molecular dynamics simulations .....	5
2.1.1 Ultrasonic measurements .....	5
2.1.2 Spectroscopy methods.....	6
2.1.3 Dielectric measurements.....	7
2.1.4 Differential scanning calorimetry .....	8
2.1.5 Nuclear magnetic resonance .....	8
2.1.6 Applicability of MD in predicting NDT responses .....	9
2.2 Ultrasonic technique .....	10
3. Results.....	11
3.1 Applicability of MD simulations in interpreting non-destructively measured data .....	12
4. Conclusions .....	16
References.....	16

## 1. Introduction

---

Cables are used in nuclear power plants (NPP) as part of instrumentation and electrical equipment to supply electricity or signal transfer. Typical estimates are that a single NPP has such cables approximately 1000-2000 km within them [Yamamoto et al.2009, Simmons et al. 2013, OECD NEA, 2011]. The cable structure consists of metallic conductor or optic fibre, insulator, possible metallic shielding and jacket as shown in Figure 1. The metallic conductor or optic fibre conducts electricity or transfers the signal. The insulator is used to electrically insulate the conductor from its environment, preventing grounding of the conductor. Additional metal shielding can be applied on the insulator to decrease outer disturbances that could affect the signal quality. The outer jacket protects the cable from external stressors.

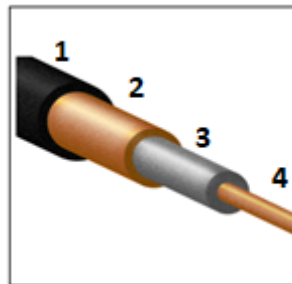


*Figure 1. Schematic illustration on the structure of the cable: (1) jacket, (2) shielding, (3) insulator and (4) conductor.*

The degradation of the insulator is commonly considered the most interesting part of the cable structure since its insulating properties ensure proper cable functionality. The main ageing mechanism related to the polymer degradation in nuclear application is radiation or thermally induced oxidation which yields in polymer chain scission, crosslinking and formation of oxidation products, such as carbonyls and hydroperoxides [IAEA, 2102]. The actual chemical reactions that govern the degradation can be quite complex in nature. They will ultimately yield in degradation of the functional properties of the polymer, e.g. electrical insulation.

Condition monitoring methods are used as part of ageing management of cables to improve the overall safety of the operating NPPs. The importance of having a properly functioning ageing management programme is emphasized when the operation licences of running NPPs are planned to be extended from the originally designed 40 year period. Condition monitoring methods are usually divided in destructive and non-destructive ones. Elongation at break is one destructive property which use has become rather well established and the general consensus is currently that 50% of the absolute elongation at break can be used as an acceptance criterion for cable insulator and jacket materials. However, using a destructive technique would require removal of the measured cable (which can be a complex operation [OECD NEA, 2011]) or use of surveillance samples which both limit the applicability of destructive techniques. Thus defining cable condition by the means of non-destructing methods would be advantageous.

Several material properties, e.g. electrical, chemical or mechanical, can be measured non-destructively. However, it is not clear how these measured material properties correlate with the cable condition. One approach how to estimate these correlations would be studying how the polymer structure evolves as function of ageing and compare it to how the measured non-destructive parameters change. In addition to experimental methods, computational tools, such as molecular dynamics (MD) simulations, can be used to assess ageing induced changes in polymer structures. It has been already shown how the crystallization of a cross linked semi-crystalline polymer system evolves during undercooling by applying MD simulations [Paajanen et al. 2019]. This report is a part of a study which aims to produce a

reliable condition monitoring method for NPP cables. As part of the study, MD simulations are applied in studying the applicability of certain non-destructive techniques (NDT) in ageing management of cables. MD is a convenient tool when the ageing of polymer systems is studied. Possibilities with the method are various, but in this context we are interested in studying:

- 1) Evolution of non-destructively measured material parameters as function of ageing.
- 2) How well they can be simulated with MD.
- 3) Whether the use of MD enables drawing correlations between material condition and the measured NDT parameters.

Understanding such relations would ease setting acceptance criterion for polymer components (to be more specific in this case, to cable insulator materials). As part of this report, screening of NDTs is conducted based on their applicability with MD simulations, i.e. how well MD simulations can predict the NDT responses in the chosen model material, cable insulator prepared from XLPE.

## 2. Methods

---

### 2.1 Molecular dynamics simulations

There are several non-destructive methods whose output data can be interpreted using MD simulations. These include

- ultrasonic measurements, which could be correlated with the simulated mechanical response to small deformations,
- spectroscopy methods that probe the energy spectrum of many-body systems at atomistic level, such as infrared and Raman spectroscopies,
- dielectric measurements, which are directly related to electrical cable performance,
- micro-sampling based differential scanning calorimetry (DSC), which provides specific heat capacities and enthalpies of reaction, and
- nuclear-magnetic resonance (NMR), which could be correlated with simulated molecular mobilities.

#### 2.1.1 Ultrasonic measurements

In solids, sound waves can generate volumetric deformations in longitudinal and transverse directions to the direction of wave propagation. For longitudinal waves, the speed of sound,  $V_L$ , is given by [Kino 1987]

$$V_L = \sqrt{\frac{E(1-\nu)}{\rho(1+\nu)(1-2\nu)}} \quad (1)$$

where  $E$ ,  $\nu$ , and  $\rho$  are Young's modulus, Poisson's ratio, and density, respectively. These material properties can be obtained from MD simulations using various simulation strategies [Shenogina et al. 2013, Vu-Bac et al. 2014], mostly involving small uniaxial deformations in

the elastic region. Effects of ageing can be readily taken into account [Ding et al. 2012]. It is also possible to make use of the bulk modulus  $K$  through expression

$$K = \frac{E}{3(1 - 2\nu)} \quad (2)$$

since determining bulk modulus from MD is both straightforward and accurate.

An alternative approach involves combining MD simulations with macroscopic conservation laws dealing with the propagation of a shock front in the material [Reed et al. 2003]. In this approach, the MD simulation cell volume and temperature are varied such that the system is constrained to the Rayleigh line and shock Hugoniot (momentum and energy conservation in the shock regime, respectively). When the particle velocities  $u_p$  behind the shock front are plotted against shock velocity  $u_s$ , a linear (or quasi-linear) relation emerges:

$$u_s = c_0 + s \cdot u_p \quad (3)$$

where  $c_0$  is the bulk speed of sound in the material, and  $s$  is a fitting parameter. Shock wave simulations could also be done by giving a large initial velocity for atoms at one edge of the cell [Xie et al. 2016] provided the system is non-periodic in the direction of the shock wave propagation.

### 2.1.2 Spectroscopy methods

MD simulations inherently describe the vibrational movements of an atomistic system, making MD a suitable tool for calculating various vibrational spectra. Crucially, the quality of these simulations depends on the force field used. To gain insight into the importance of the potential, it is instructive to consider an equilibrium structure of atoms at positions  $x_i$ . The potential energy described by the force field can be expanded as a Taylor series considering small displacements around equilibrium positions [Soldara and Dognon 1997]

$$V = V_0 + \sum \left( \frac{\partial V}{\partial x_i} \right) x_i + \sum \left( \frac{\partial^2 V}{\partial x_i \partial x_j} \right) x_i x_j + O(x^3). \quad (4)$$

In equilibrium  $V_0$  can be set to zero, and the first gradient term disappears. For small displacements, third-order terms can be neglected (harmonic approximation). The remaining second-order derivatives describe the vibrational normal modes of the system, and they can be computed using the analytical expression for the force field.

The complete vibrational spectrum of the system is obtained from MD simulations as the Fourier transform of the velocity autocorrelation function:

$$\Phi(\omega) = \frac{1}{2\pi} \int_{-\infty}^{\infty} \langle v(t)v(0) \rangle e^{-i\omega t} dt. \quad (5)$$

IR and Raman spectroscopies are sensitive to subsets of this vibrational spectrum. In MD, the IR spectrum is obtained from the autocorrelation function of dipole moment  $\mathbf{M}$  as [Wang et al. 2017]

$$I_{IR}(\omega) = \frac{1}{2\pi} \int_{-\infty}^{\infty} \langle \mathbf{M}(t)\mathbf{M}(0) \rangle e^{-i\omega t} dt, \quad (6)$$

and the absorption coefficient  $\alpha(\omega)$  is

$$\alpha(\omega)n(\omega) = \frac{4\pi^2\omega^2}{3Vck_B T} I_{IR}(\omega), \quad (7)$$

where  $n(\omega)$  is the refractive index of the material.

The isotropic and anisotropic parts of the Raman spectrum can be gained from the autocorrelation function of polarizability tensor  $\mathbf{A}$  as [Wang et al. 2017]

$$I_{Raman}^{Iso}(\omega) = \frac{1}{2\pi} \int_{-\infty}^{\infty} \langle \bar{A}(t)\bar{A}(0) \rangle e^{-i\omega t} dt, \quad (8)$$

$$I_{Raman}^{Aniso}(\omega) = \frac{1}{2\pi} \int_{-\infty}^{\infty} \langle Tr(\mathbf{B}(t)\mathbf{B}(0)) \rangle e^{-i\omega t} dt, \quad (9)$$

where  $\bar{A}=(1/3)Tr(\mathbf{A})$  is the isotropic part of the polarizability tensor  $\mathbf{A}$ , and  $\mathbf{B}=\mathbf{A}-\bar{A}\mathbf{I}$  is the traceless anisotropic part of the polarizability. The intensity of the Raman scattering for polarization parallel to the incident radiation is

$$I_{Raman}^{\parallel}(\omega) = \left[ \frac{n}{c}(\omega_0 - \omega) \right]^4 \frac{h\omega}{2\pi k_B T} \left( \frac{1}{1 - e^{-h\omega/2\pi k_B T}} \right) \left( I_{Raman}^{Iso}(\omega) + \frac{2}{15} I_{Raman}^{Aniso}(\omega) \right). \quad (10)$$

Classical MD is expected to give only a qualitative description of the vibrational spectra due to the fact that it cannot adequately treat anharmonic effects. The use of Ab-Initio MD (AIMD), where electronic structure is computed using quantum mechanics, overcomes these restrictions [Thomas et al. 2013], while significantly increasing the computational cost, and requiring advanced methods to obtain dipole moments and polarizabilities. As a possible remedy, machine-learning potentials for accelerating AIMD calculations have been proposed [Gastegger et al. 2017].

### 2.1.3 Dielectric measurements

If an external electric field is applied to the system, the zero-frequency (static) permittivity  $\epsilon(0)$  can be computed from the average dipole moment. Assuming the external field  $E_{ext}^z$  is along z-axis, we have [Riniker et al. 2011]

$$\epsilon(0) = 1 + 4\pi \frac{\langle M_z \rangle}{VE_{ext}^z}, \quad (11)$$

where  $\langle M_z \rangle$  is the average dipole moment in volume  $V$  in the z-direction. In absence of an external electric field, the relative permittivity can be computed as [Misra et al. 2014]

$$\epsilon_r = \epsilon_\infty + \frac{4\pi(\langle M^2 \rangle - \langle M \rangle^2)}{3Vk_B T}, \quad (12)$$

where  $M$  is the total dipole moment in volume  $V$ .

The calculation of the complex, frequency-dependent dielectric permittivity is based on the normalized autocorrelation function of the dipole moment:

$$\Phi(t) = \frac{\langle M(t)M(0) \rangle}{\langle M(0)M(0) \rangle}. \quad (13)$$

The complex dielectric permittivity  $\epsilon(i\omega) = \epsilon'(\omega) - i\epsilon''(\omega)$  is obtained from [Misra and Kumar 2017]

$$\frac{\epsilon(i\omega) - \epsilon_\infty}{\epsilon_0 - \epsilon_\infty} = \int_0^\infty \left[ -\frac{d\Phi(t)}{dt} \right] e^{-i\omega t} dt. \quad (14)$$

The real and complex components can be separated as [Jämbeck et al. 2015]

$$\frac{\epsilon'(\omega) - \epsilon_\infty}{\epsilon_0 - \epsilon_\infty} = \int_0^\infty \left[ -\frac{d\Phi(t)}{dt} \right] \cos(\omega t) dt \quad (15)$$

and

$$\frac{\epsilon''(\omega)}{\epsilon_0 - \epsilon_\infty} = \int_0^\infty \left[ -\frac{d\Phi(t)}{dt} \right] \sin(\omega t) dt \quad (16)$$

allowing the calculation of the dissipation factor  $\tan \delta$  through

$$\tan \delta = \frac{\epsilon''}{\epsilon'}. \quad (17)$$

#### 2.1.4 Differential scanning calorimetry

When a sample material is subjected to a linear temperature program, the heat flow rate into the sample is proportional to its instantaneous specific heat

$$\frac{dH}{dt} = mC_p \frac{dT}{dt}. \quad (18)$$

In a DSC [Watson et al. 1964, O'Neill 1966], the measurement of  $C_p$  involves heating two identical sample holders using a linear temperature programme, with the sample placed in one of them, and with the other being either empty or containing a well-known reference sample (such as sapphire). The heat required to maintain the two sample holders at the same temperature is recorded. In addition to  $C_p$ , the measurement is sensitive to phase transitions such as glass transition, crystallisation, and melting.

In MD, it is possible to apply eq. (18) directly by heating the system linearly and recording enthalpy during the simulation, or by recording time-averaged enthalpies at several constant temperatures. Another possibility is to make use of the fluctuations observed in enthalpy, in which case  $C_p$  can be obtained from [Mayorga et al. 1988]

$$C_p = \frac{\overline{H^2} - (\overline{H})^2}{RT^2}. \quad (19)$$

When the system is heated using a linear temperature ramp, and a phase transition temperature (such as melting) is crossed, it is possible to integrate the resulting  $C_p$ -T curve to obtain the reaction enthalpy of the phase transition. Comparison to the heat of fusion of a fully crystalline sample allows determination of the degree of crystallinity. An example on this is provided by [Ramos et al. 2015] for polyethylene crystallization.

#### 2.1.5 Nuclear magnetic resonance

Nuclear magnetic resonance is the measurement of the oscillating magnetic field produced by atomic nuclei which have been perturbed by an external oscillating magnetic field. The frequency of the field produced by the nuclei is sensitive to the chemical environment of the

nuclei. A chemical shift is the resonant frequency of a nucleus relative to a standard in a magnetic field. Chemical shifts can be used to identify structures of chemical compounds. Sometimes, especially if the molecule is complex, this assignment can be corroborated by performing an MD simulation of the same system and comparing the structures predicted by NMR and MD [Asakura et al. 2018]. The MD simulation itself does not provide chemical shifts. They can be calculated from the predicted structures using additional software packages such as SHIFTX2 [Han et al. 2011].

When the external perturbing magnetic field is removed, the magnetic field produced by the nuclei starts to decay as a function of time. Measuring and analyzing the Free Induction decay (FID) characteristics of the magnetic field provides information on the mobility of the nuclei, and therefore the molecules they are part of. There are two main relaxation mechanisms, and accordingly, two characteristic relaxation times:  $t_1$  (spin-lattice) and  $t_2$  (spin-spin) that can provide detailed information on the mobility of polymer molecules and segments thereof [Bärenwald et al. 2014, Trutschel et al. 2018]. Conversely, it is also possible to compute NMR relaxation times from MD simulations [Singer et al. 2018].

### 2.1.6 Applicability of MD in predicting NDT responses

The previously discussed NDTs were estimated and compared among themselves in order to identify how well the related material parameters could be predicted by using MD simulations. The summary of this comparison is presented in Table 1. Summary on the applicability of MD simulations to predict various NDT parameters. IR/Raman spectroscopy parameters seemed to be the most challenging ones to be predicted by using MD. This is due to limited ability of MD to produce the vibrational spectra. Similarly, NMR parameters can be considered to somewhat challenging to produce because the chemical shifts cannot be directly predicted by MD. DSC and dielectric spectroscopy seemed to be more easily interpreted than IR/Raman spectroscopy and NMR, since the two later mentioned techniques would require application of additional modelling methods (Ab-Initio MD, AIMD, SHIFTX2) in order to obtain qualitatively accurate results. Ultrasonic measurement parameters were concluded to be the most easy to be simulated with MD as there were several different methods to extract the NDT parameters, some of them being rather straightforward and accurate.

Table 1. Summary on the applicability of MD simulations to predict various NDT parameters.

Technique	Measured parameter	Applicability with MD simulations
DSC	Reaction enthalpy, specific heat capacity	Easy to moderate
Infrared / Raman spectroscopy	Vibrational movement of functional groups	Hard
NMR	Relaxation time (phase composition and dynamics of polymer chains)	Moderate to hard
Ultrasonic	Young's modulus, Poisson's ratio, and density	Easy
Dielectric spectroscopy	Permittivity and dielectric loss	Easy to moderate

## 2.2 Ultrasonic technique

As it seems that the ultrasonic parameters are the most easily accessible by MD, in the following the basics of ultrasonic measurement are introduced. Sound velocity can be measured by using traditional pulse-echo technique. In this method, the time-of-flight and the sound-path are measured separately. The sound velocity is then calculated as the ratio of the sound-path and the time of flight (TOF):

$$\text{sound velocity} = \frac{\text{sound path length}}{\text{time of flight}} \quad (20)$$

The thickness of the measured plate sample is assumed to be the sound path length.

A schematic illustration on the ultrasonic measurement setup is shown in **Error! Reference source not found.** A pulser-receiver with suitable sampling rate (e.g. 100 MHz) is used to generate electrical pulses that are converted by the transducer into ultrasonic pulses. These pulses travel through the delay line, which is typically piezoelectric crystals that cause a precise time delay in the propagating signal, over the probe-sample interface. On the sample surface, a contact agent is applied in order to improve the contact between the probe and the sample. At the back end of the sample, the signal is reflected back through the same route all the way back to the pulser-receiver. The TOF can be calculated from the measurement signal, of which an example is shown in **Error! Reference source not found.** The time difference between front wall echo and second back wall echo is typically used in the calculation of the TOF. It is notable that this time difference is four times the actual TOF.

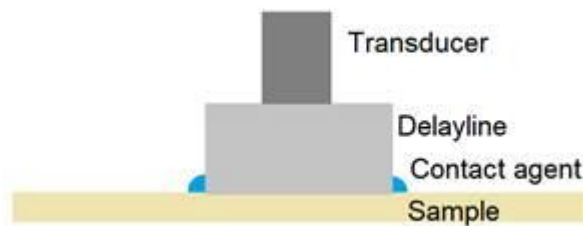


Figure 2. Schematic illustration on the measurement setup for time of flight measurement.

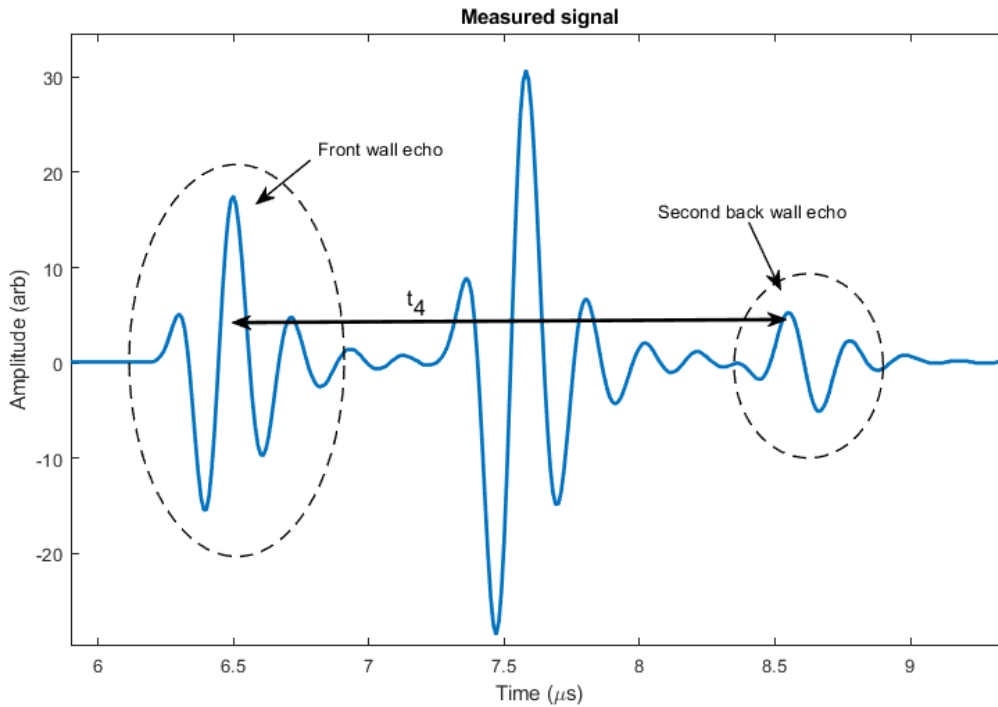


Figure 3. An example of a measured ultrasound signal. The time difference between front wall echo and the second back wall echo is four times the actual time of flight.

As mentioned, the sound velocity can be calculated using equation (20). If the TOF is measured using the second back wall echo, the thickness has to be multiplied by factor of four. Using the standard deviation of the mean, the actual sound path length can be presented as  $4s \pm 2\Delta s$ . Thus the actual velocity and corresponding standard deviation can be calculated by using equation:

$$v \pm \Delta v = \frac{4s}{t_4} \pm \frac{4s}{t_4} \sqrt{\left(\frac{2\Delta s}{s}\right)^2 + \left(\frac{\Delta t_4}{t_4}\right)^2} \quad (21)$$

where  $s$  is the measured thickness of the plate and  $\Delta s$  is the corresponding standard deviation. Time difference between front wall echo and second back wall echo is  $t_4$  and  $\Delta t_4$  is the measurement error in the time measurement. Using the second back wall echo instead of the first one reduces the relative error in velocity calculations significantly.

### 3. Results

Based on the previous screening, the potential of MD simulations in interpreting ultrasound measurements is investigated in more detail. The methods for setting up the required polymer structures and MD simulations are similar to those reported in [Paajanen et al. 2019].

### 3.1 Applicability of MD simulations in interpreting non-destructively measured data

The model PE and XLPE systems consisted of 900 chains with 1000 CH<sub>2</sub> repeat units each. For each structure, first an amorphous melt was generated at a reference temperature of 600 K using an in-house chain packing algorithm. This initial structure was then equilibrated by running MD at 600 K until chain conformations and chain entanglement density reached steady-state values, typically within 300 ns. For XLPE model systems, chemical cross-linking was performed after equilibration to reach a target gel fraction. This was followed by cooling to 300 K and crystallization at 300 K for up to 2 μs, which yielded a crystallinity of about 47 % for PE and about 40% for XLPE (at gel fraction of 0.71). The corresponding final densities were 924 kg/m<sup>3</sup> (PE) and 917 kg/m<sup>3</sup> (XLPE). The crystalline phase of the final PE structure is shown in Figure 4. The number of randomly oriented crystallites is 48.

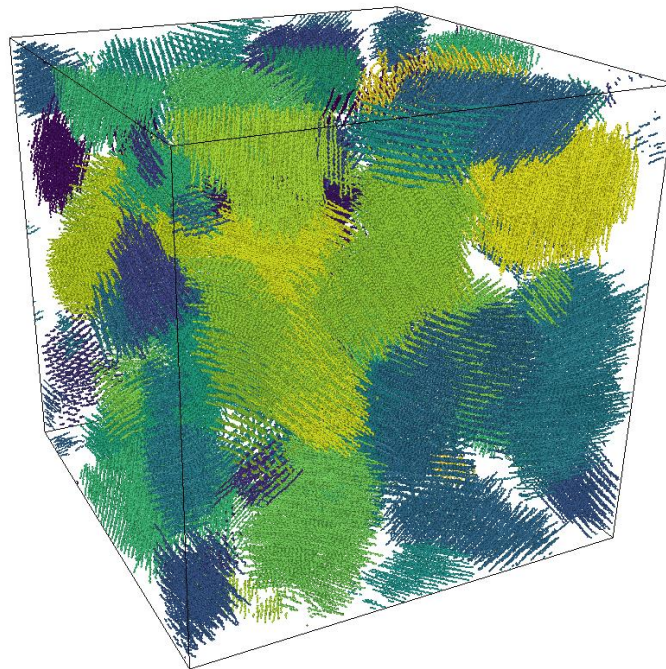


*Figure 4. Crystallites formed in a linear PE system of 900 chains with 1000 CH<sub>2</sub> repeat units each after 2 μs of crystallization at 300 K.*

One way of using MD to obtain Young's modulus and Poisson's ratio, required along density to calculate the speed of sound, is to mimic the standard tensile test. This is done by uniaxially deforming the simulation box, while applying zero-pressure boundary conditions in the two perpendicular directions to allow the structure to freely conform to the deformed box. During the simulation, the stress in the deformed direction, as well as the box dimensions, are recorded.

Figure 5 presents stress-strain curves for the PE and XLPE systems at strain rates of 10<sup>6</sup> 1/s and 10<sup>7</sup> 1/s. The curves are presented both as logarithmic (true stress vs true strain) and linear (engineering stress vs engineering strain) plots. The initial increase of the curves is not perfectly linear, reflecting the viscoelastic nature of polymers. Yielding occurs in a strain range of about 0.1-0.2, after which gradual strain hardening is observed. The fact that the magnitude of the stress depends on strain rate is another indication of the viscoelastic behaviour. The initial slope for the same strain rate is nearly the same for PE and XLPE. Note that the strain rates used in MD are several orders of magnitude higher than in real-life tensile tests, due to computational limitations. The curves are in semi-quantitative agreement with those measured

by several authors [Crist et al. 1989, Kennedy et al. 1994, Krishnaswamy and Lamborn 2000, Jar 2015].

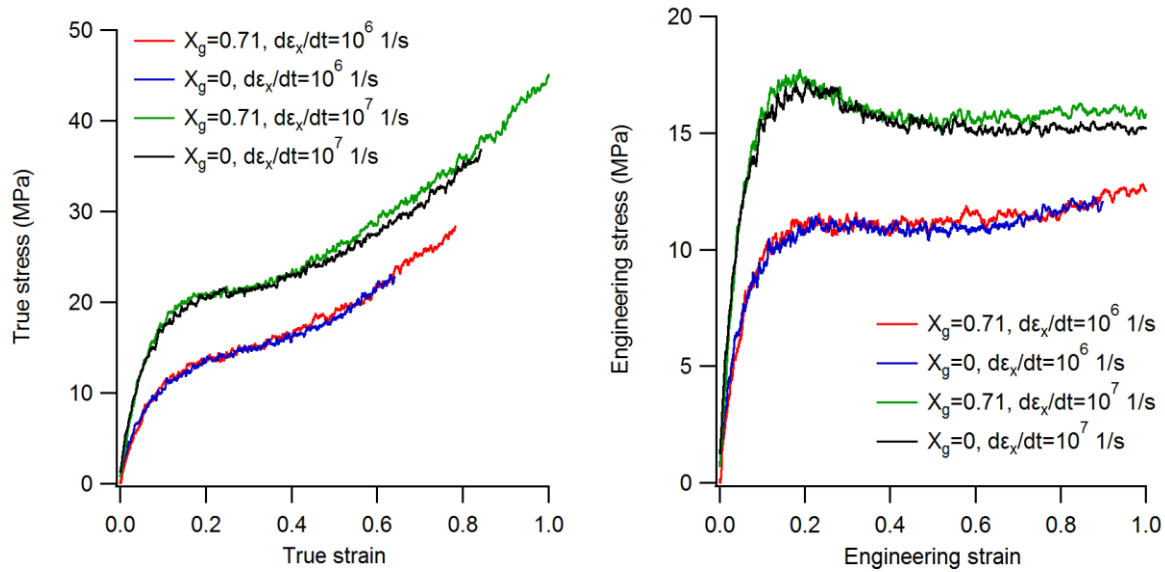


Figure 5. Simulated stress-strain curves for the PE (blue and black curves) and XLPE (red and green curves) systems.  $X_g$  stands for gel fraction, and  $d\epsilon_x/dt$  for strain rate in x direction.

Young’s modulus is determined from a stress-strain curve as the slope of a line fitted to the initial part of the curves. The simulated curves in Figure 6 for the XLPE system are averages over strain applied in x-, y-, and z- directions separately. Linear fits give  $E=297$  MPa and  $E=172$  MPa for strain rates  $10^7$  and  $10^6$  1/s, respectively. The same procedure for the PE system results in  $E=304$  MPa and  $E=180$  MPa, for strain rates  $10^7$  and  $10^6$  1/s, respectively. These values fall in the range of moduli reported in [Crist et al. 1989, Kennedy et al. 1994, Krishnaswamy and Lamborn 2000, Jar 2015]. More specifically, [Crist et al. 1989] reports a linear dependence of  $E$  on density, and from Figure 2 of [Crist et al. 1989] a density on  $920$   $\text{kg/m}^3$  approximately corresponds to  $E=150$  MPa. Assuming densities of  $1003$   $\text{kg/m}^3$  for crystalline PE and  $850$   $\text{kg/m}^3$  for amorphous PE, this corresponds to a crystallinity of 47.6 %. In Figures 16-18 of [Kennedy et al. 1994], a linear dependence of  $E$  on crystallinity is reported. The paper makes a distinction between core crystallinity and crystallinity determined based on density, with core crystallinity corresponding closely to the crystallites identified in this work from MD structures. Core crystallinity around 40% corresponds to  $E$  of about 150 MPa. These data suggest that the MD results from the lower strain rate of  $10^6$  1/s are more physically correct.

Poisson’s ratio may be determined from the same simulations by using the recorded box dimensions and directly applying the definition

$$\nu = -\frac{d\epsilon_{\text{transverse}}}{d\epsilon_{\text{axial}}}. \tag{n}$$

The practical problem is associated with the fluctuations of the transverse box dimensions due to barostatting and finite system size, reducing the accuracy of the calculation. In this work,  $\nu$  was calculated as a running average over the entire data with  $d\epsilon_{\text{axial}}$  chosen as 0.004 (strain rate  $10^7$  1/s) or 0.0004 (strain rate  $10^6$  1/s), and finally averaging the values over three directions. The Poisson’s ratios for PE were  $\nu(10^7$  1/s)=0.480662 and  $\nu(10^6$  1/s)=0.483732, and for XLPE  $\nu(10^7$  1/s)=0.474657 and  $\nu(10^6$  1/s)=0.48556.

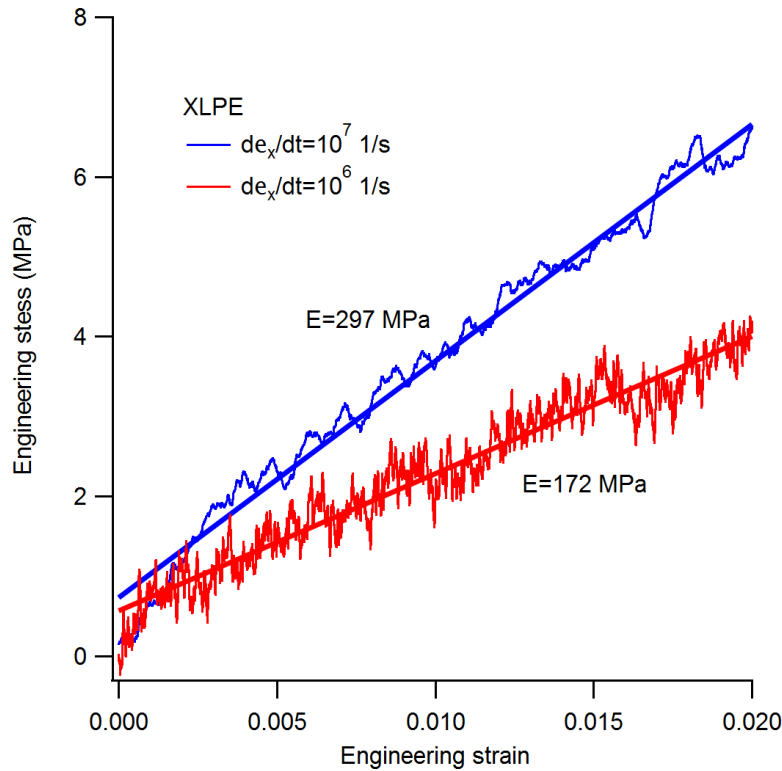


Figure 6. Determination of the Young's modulus for the XLPE system.

Another way of obtaining Poisson's ratio is when both bulk modulus  $K$  and Young's modulus  $E$  of a material are known. Then, Poisson's ratio may be calculated from

$$\nu = \frac{3K - E}{6K}. \tag{n}$$

Bulk modulus can be easily calculated in MD by isotropically compressing the material and recording the box dimensions as a function of applied pressure. The resulting  $V(p)$  data can then be used to compute  $K$  directly from the definition

$$K = -V \frac{dp}{dV}. \tag{n}$$

In the simulations, pressure was increased from zero to 1000 atm, which resulted in about 3.3 % reduction of the box volume. This approach yields bulk moduli of 2.75 GPa and 2.64 GPa for PE and XLPE, respectively. Using the Young's moduli obtained above, the Poisson's ratios for PE and XLPE become  $\nu(\text{PE})=0.481576$  and  $\nu(\text{XLPE})=0.48125$ .

Sound velocities calculated using Eq. (1) based on the MD data above are summarized in Table 2.

Table 2. Sound velocities for PE and XLPE calculated based on the MD data.

Material	$\rho$ (kg/m <sup>3</sup> )	$d\varepsilon/dt$ (1/s)	E (MPa)	$\nu$	$v$ (m/s)
PE	924	$10^7$	304	0.480662 <sup>a</sup>	1727
				0.481576 <sup>b</sup>	1768
		$10^6$	180	0.483732 <sup>a</sup>	1443
				0.481576 <sup>b</sup>	1360
XLPE	917	$10^7$	297	0.474657 <sup>a</sup>	1509
				0.481250 <sup>b</sup>	1739
		$10^6$	172	0.485560 <sup>a</sup>	1500
				0.481250 <sup>b</sup>	1324

a) from tensile data

b) from bulk modulus

The sound velocities in Table 2 are generally low compared to literature values. Sinha and Buckley [Sinha and Buckley 2007] list a longitudinal sound velocity of 2430 m/s for linear PE (957 kg/m<sup>3</sup>, 1 MHz, 25 °C). Rae and Brown [Rae and Brown 2015] report longitudinal sound velocities between 2573 and 2628 m/s for HDPE (crystallinity 80.9 %, density 970 kg/m<sup>3</sup>) and between 2141 and 2173 m/s for UHMWPE (crystallinity 38.6%, density 927 kg/m<sup>3</sup>), both at 21 °C and 5 MHz. Buchholz et al. [Buchholz et al. 2011] measured the temperature dependence of the longitudinal sound velocity for XLPE taken from a 400 kV high voltage cable, and found values from 2331 m/s at -20 °C to 1744 m/s at 50.5 °C.

It is especially noteworthy that the more physical, lower E values from the lower strain rate produce worse sound velocity predictions compared to experimental data. No adequate explanation for this can be given at this point. It can be noted however that Eq. (1) for sound velocity is very sensitive to the value of  $\nu$  when  $\nu$  is close to 0.5. Further work to develop an accurate method to determine  $\nu$  is required. It is also possible that the TraPPE interaction potential used in the simulations is a source of inaccuracy.

For the MSST simulations, the *fix msst* command implemented in LAMMPS software was used. Shock velocities were varied from 2.0 km/s to 3.0 km/s, which resulted in simulation box compressing 4.6% to 16 % in the direction of shock wave propagation. The resulting particle velocity data, averaged over three directions, is plotted in Figure 7 for linear PE. The data has been fitted with a second-order polynomial, which is required to capture the slight curvature of the data. Such a curvature has also been observed in experiments [Lässig 2015] which give a sound velocity of 1892 m/s for linear polyethylene. The intercept of the curve with y-axis gives a sound velocity of 1767 m/s. Similar procedure for XLPE yields a sound velocity of 1717 m/s. These values are at the upper range of the values tabulated in Table 2.

In summary, it has been shown that it is possible to derive mechanical parameters (density, Young's modulus, Poisson's ratio and bulk modulus) from molecular dynamics simulations in order to calculate an estimate for the longitudinal velocity of sound in PE and XLPE. The sound velocity estimates obtained in this work are however lower than values measured experimentally, and further work is required to understand the underlying reasons. Further work is also required to investigate whether changes in sound velocity estimates due to aging effects in PE and XLPE can be simulated. This will be included as part of the future work in 2020.

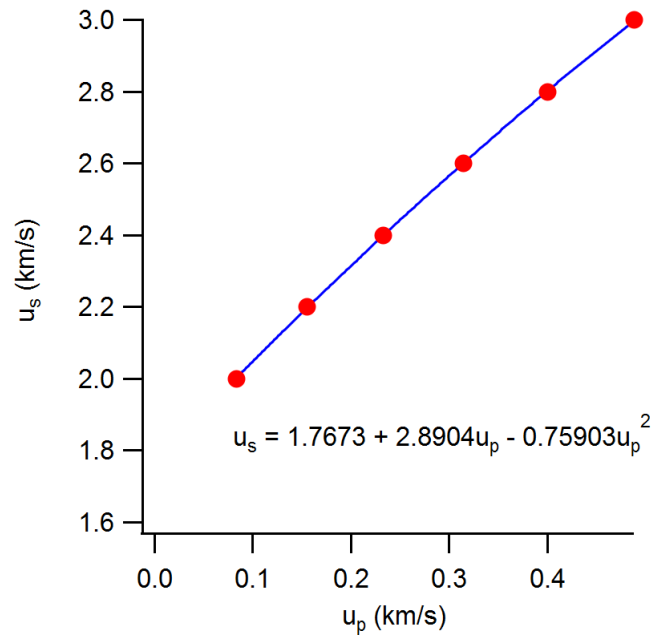


Figure 7. Simulated shock velocity data for linear PE.

## 4. Conclusions

Various potential NDTs for NPP cable ageing management were estimated whether their measurement parameters could be predicted by using MD simulations. From the first screening, ultrasonic technique seemed to be the most compatible with MD simulations. The performed MD simulations showed that the parameters required for sound velocity calculation, i.e. Young's modulus, Poisson's ratio and density values, could be extracted for PE and XLPE by mimicking standardized tensile test. However, the obtained values were lower than the ones reported in the literature. This may be due to the sensitivity of the sound velocity to certain parameters, such as the Poisson's ratio. The future work will focus on examining the inconsistency between the calculated and in the literature reported sound velocity values and providing data how ageing affects to the sound velocity values.

## References

- Asakura, T., Nishimura, A. and Tasei, Y. 2018. Determination of Local Structure of  $^{13}\text{C}$  Selectively Labeled 47-mer Peptides as a Model for Gly-Rich Region of Nephila clavipes Dragline Silk Using a Combination of  $^{13}\text{C}$  Solid-State NMR and MD Simulation. *Macromolecules* vol. 51 pp. 3608-3619.
- Buchholz, U., Jaunich, M., Stark, W., Habel, W. and Petersson, B.A.T. 2011. Acoustic Data of Cross linked Polyethylene (XLPE) and Cured Liquid Silicone Rubber (LSR) by Means of Ultrasonic and Low Frequency DMTA. *IEEE Transactions on Dielectrics and Electrical Insulation* vol. 19 pp. 558-566.
- Bärenwald, R., Goerlitz, S., Godehardt, R., Osichow, A., Tong, Q., Krumova, M., Mecking, S. and Saalwächter, K. 2014. Local Flips and Chain Motion in Polyethylene Crystallites: A Comparison of Melt-Crystallized Samples, Reactor Powders, and Nanocrystals. *Macromolecules* vol. 47 pp. 5163-5173.

- Crist, B., Fisher, C.J. and Howard, P.R. 1989. Mechanical Properties of Model Polyethylenes: Tensile Elastic Modulus and Yield Stress. *Macromolecules* vol. 22 pp. 1709-1718.
- Ding, L., Davidchack, R.L. and Pan, J. 2012. A molecular dynamics study of Young's modulus change of semi-crystalline polymers during degradation by chain scissions. *Journal of the Mechanical Behavior of Biomedical Materials* vol. 5 pp. 224-230. <https://doi.org/10.1016/j.jmbbm.2011.09.002>
- Gastegger, M., Behler, J. and Marquetand, P. Machine learning molecular dynamics for the simulation of infrared spectra. *Chemical Science* vol. 8 pp. 6924-6935. <https://doi.org/10.1039/c7sc02267k>
- Han, B., Liu, Y., Ginzinger, S.W. and Wishart, D.S. 2011. SHIFTX2: significantly improved protein chemical shift prediction. *Journal of Biomolecular NMR* vol. 50 pp. 43-57.
- IAEA. 2012. Assessing and Managing Cable Ageing in Nuclear Power Plants. Technical report. 111 pp.
- Jar, P.-Y.B. 2015. Effect of Tensile Loading History on Mechanical Properties for Polyethylene. *Polymer Engineering and Science* vol. 55 pp. 2002-2010. <https://doi.org/10.1002/pen.24042>
- Jämbeck, J.P.M., Unge, M. and Laihonon, S. 2015. Determining the Dielectric Losses in Polymers by Using Molecular Dynamics Simulations. Annual Report - Conference on Electrical Insulation and Dielectric Phenomena (CEIDP 2015) pp. 146-149. <https://docplayer.net/45214454-2015-ieee-conference-on-electrical-insulation-and-dielectric-phenomena-ceidp-2015.html>
- Kennedy, M.A., Peacock, A.J. and mandelkern, L. 1994. Tensile Properties of Crystalline Polymers: Linear Polyethylene. *Macromolecules* vol. 27 pp. 5297-5310.
- Kino, G. 1987. Acoustic Waves: Devices, Imaging, and Analog Signal Processing. Section 2.2. Basic Theory for Waves in Isotropic Media. Prentice-Hall Signal Processing Series. ISBN-13: 978-0130030474
- Krishnaswamy, R.K. and Lamborn, M.J. 2000. Tensile Properties of Linear Low Density Polyethylene (LLDPE) Blown Films. *Polymer Engineering and Science* vol. 40 pp. 2385-2396.
- Lässig, T., Bagusat, F., May, M. and Hiermaier, S. 2015. Analysis of the shock response of UHMWPE composites using the inverse planar plate impact test and the shock reverberation technique. *International Journal of Impact Engineering* vol. 86 pp. 240-248. <http://dx.doi.org/10.1016/j.ijimpeng.2015.08.010>
- Mayorga, O.L., van Osdol, W.W., Lacomba, J.L. and Freire, E. 1988. Frequency spectrum of enthalpy fluctuations associated with macromolecular transitions. *Proceedings of the National Academy of Sciences of the United States of America* vol. 85 pp. 9514-9518.
- Misra, M., Agarwal, M., Sinkovits, D.W., Kumar, S.K., Wang, C., Pilia, G., Ramprasad, R., Weiss, R.A., Yuan, X. and Chung, T.C.M. 2014. Enhanced Polymeric Dielectrics through Incorporation of Hydroxyl Groups. *Macromolecules* vol. 47 pp. 1122-1129. <http://dx.doi.org/10.1021/ma402220j>
- OECD NEA. 2011. TECHNICAL BASIS FOR COMMENDABLE PRACTICES ON AGEING MANAGEMENT - SCC and Cable Ageing Project (SCAP). Final Report. 132 pp.

- O'Neill, M.J. 1966. Measurement of Specific Heat Functions by Differential Scanning Calorimetry. *Analytical Chemistry* vol. 38 pp. 1331-1336. <http://web.iitd.ac.in/~nkurur/2010-11/lsem/cyl501/dsc2.pdf> (retrieved 15.11.2019)
- Paajanen, A., Vaari, J. and Verho, T. 2019. Crystallization of cross-linked polyethylene in molecular dynamics simulation. *Polymer* vol. 171 pp. 80-86. <https://doi.org/10.1016/j.polymer.2019.03.040>
- Rae, P.J. and Brown, E.N. 2015. Some Observations on Measuring Sound Speeds in Polymers Using Time-of-Flight. *Experimental Techniques* vol. 40 pp. 1085-1097. <https://doi.org/10.1007/s40799-016-0109-6>
- Ramos, J., Vega, J.F. and Martinez-Salazar, J. 2015. Molecular Dynamics Simulations for the Description of Experimental Molecular Conformation, Melt Dynamics, and Phase Transitions in Polyethylene. *Macromolecules* vol. 48 pp. 5016-5027. <https://doi.org/10.1021/acs.macromol.5b00823>
- Reed, E.J., Fried, L.E. and Joannopoulos, J.D. 2003. A Method for Tractable Dynamical Studies of Single and Double Shock Compression. *Physical Review Letters* vol. 90 article no 235503. <https://doi.org/10.1103/PhysRevLett.90.235503>
- Riniker, S., Kunz, A.-P.E. and van Gunsteren, W.F. 2011. On the Calculation of the Dielectric Permittivity and Relaxation of Molecular Models in the Liquid Phase. *Journal of the Chemical Theory and Computation* vol. 7 pp. 1469-1475. <http://dx.doi.org/10.1021/ct100610v>
- Shenogina, N.B., Tsige, M., Patnaik, S.S. and Mukhopadhyay, S.M. 2013. Molecular modeling of elastic properties of thermosetting polymers using a dynamic deformation approach. *Polymer* vol. 54 pp. 3370-3376. <http://dx.doi.org/10.1016/j.polymer.2013.04.034>
- Simmons, Pardini, Fifield, Tedeschi, Westman, Jones, Ramuhalli. 2013. Determining Remaining Useful Life of Aging Cables in Nuclear Power Plants – Interim Study FY13. Pacific Northwest National Laboratory. 66 pp.
- Singer, P.M., Asthagiri, D., Chen, Z., Parambathu, A.V., Hirasaki, G.J. and Chapman, W.G. 2018. Role of internal motions and molecular geometry on the NMR relaxation of hydrocarbons. *The Journal of Chemical Physics* vol. 148, 164507.
- Sinha, M. and Buckley, D.J. 2007. in: *Physical Properties of Polymers Handbook* (Mark J.E., ed.) Chapter 60 Acoustic Properties of Polymers. Springer Science. ISBN-13: 978-0-387-31235-4.
- Soldera, A. and Dognon, J.-P. 1997. Infrared absorption spectra of polymers from classical molecular simulation. *Macromolecular Symposia* vol. 119 pp. 157-164.
- Thomas, M., Brehm, M., Fligg, R., Vöhringer, P. and Kirchner, B. 2013. Computing vibrational spectra from ab initio molecular dynamics. *Physical Chemistry Chemical Physics* vol. 15 pp. 6608-6622. <https://doi.org/10.1039/C3CP44302G>
- Trutschel, M.-L., Mordvinkin, A., Furtado, F., Willner, L. and Saalwächter, K. 2018. Time-Domain NMR Observation of Entangled Polymer Dynamics: Focus on All Tube-Model Regimes, Chain Center, and Matrix Effects. *Macromolecules* vol. 51 pp. 4108-4117.
- Vu-Bac, N., Lahmer, T., Keitel, H., Zhao, J., Zhuang, X. and Rabczuk, T. 2014. Stochastic predictions of bulk properties of amorphous polyethylene based on molecular dynamics simulations. *Mechanics of Materials* vol. 68 pp. 70-84. <http://dx.doi.org/10.1016/j.mechmat.2013.07.021>

- Wang, L., Ishiyama, T. and Morita, A. 2017. Theoretical Investigation of C–H Vibrational Spectroscopy. 1. Modeling of Methyl and Methylene Groups of Ethanol with Different Conformers. *The Journal of Physical Chemistry A* vol. 121 pp. 6687-6700. <https://doi.org/10.1021/acs.jpca.7b05320>
- Watson, E.S., O'Neill, M.J., Justin, J. and Brenner, N. 1964. A Differential Scanning Calorimeter for Quantitative Differential Thermal Analysis. *Analytical Chemistry* vol. 36 pp. 1233-1238. <http://web.iitd.ac.in/~nkurur/2010-11/lsem/cyl501/dsc1.pdf> (retrieved 15.11.2019).
- Xie, F., Lu, Z., Yang, Z., Hu, W. and Yuan, Z. 2016. Mechanical behaviors and molecular deformation mechanisms of polymers under high speed shock compression: A molecular dynamics simulation study. *Polymer* vol. 98 pp. 294-304. <http://dx.doi.org/10.1016/j.polymer.2016.06.047>
- Yamamoto, Minakawa. 2009. Assessment of Cable Aging for Nuclear Power Plants. Japan Nuclear Energy Safety Organization. JNES-SS-0903 Report. 322 pp.